Dynamic-Bias S-Parameters: A New Measurement Technique for Microwave Transistors

Gustavo Avolio, *Member, IEEE*, Antonio Raffo, *Member, IEEE*, Valeria Vadalà, *Member, IEEE*, Giorgio Vannini, *Member, IEEE*, and Dominique M. M.-P. Schreurs, *Fellow, IEEE*

***Abstract*— We present the first application of the recently introduced dynamic-bias measurement to the acquisition of the scattering (S-) parameters of microwave transistors under large-signal operating conditions. We demonstrate that by properly acquiring and processing dynamic-bias measurements, one can derive the S-parameters of a nonlinear device-under test across a time-varying large-signal operating point (LSOP). Interestingly, these time-varying S-parameters can be used similar to the conventional S-parameters for characterization and modeling purposes. As compared with similar existing approaches, like those based on the pulsed S-parameter measurements, with the proposed technique, one can obtain, as a result of one measurement, the frequency-dependent S-parameters at each instantaneous point touched by the LSOP. We report experimental dynamic-bias S-parameters of a 0.15-μm GaAs pHEMT and a 0.25-μm GaN HEMT.**

***Index Terms*— Dynamic-bias, large-signal network analyzer (LSNA), microwave transistors, nonlinear measurements, S-parameters.**

I. Introduction

NONLINEAR characterization is an important step when dealing with the transistors used in the design of microwave circuits like mixers, power amplifiers, and oscillators, which typically operate under large-signal conditions. For such a reason, next to the classical dc and S-parameter transistor measurements, setups enabling vector calibrated measurements under nonlinear operation have been developed in the last 20 years. These systems, like the large-signal network analyzers (LSNA), make use of real-time scopes, harmonic samplers, and mixer-based receivers [1]–[10]. These instruments provide a great deal of information on the device behavior as they allow its characterization in conditions very close to those experienced in real-life applications. Nevertheless, performing nonlinear characterization at microwave frequencies is not always a straightforward task [11]. In the case, for instance, of harmonically tuned amplifiers, one needs to measure and tune at least three harmonics, and therefore the maximum fundamental frequency that can be used for continuous-wave (CW) measurements is limited to the instrument bandwidth divided by three. Whereas the solutions to perform scalar nonlinear measurements in the millimeter-wave frequency range do exist [12], today's limit of instrumentation enabling the vector calibrated nonlinear measurements is 67 GHz, and therefore the highest fundamental frequency, which could be used is around 22 GHz. Moreover, for harmonic-tuned amplifiers, one is interested in knowing the load line at the transistor current-generator plane, and this is not accessible at microwave frequencies. Among others, an approach to overcome some of these limitations consists in introducing low-frequency measurements in the characterization phase of microwave transistors. Several works addressing this topic have been presented in the last years, including [13]–[19]. In these works, the authors show the benefit of using low-frequency measurements for different purposes, encompassing characterization, modeling, and design. In this context, we recently proposed the dynamic-bias measurement technique [19]–[21], which combines low- and high-frequency measurements. In [19]–[21], we were driven by the need of extracting the models for transistors by using experimental data that reproduced the operating conditions as close as possible to those in real-life, but beyond the limitations of today's vector calibrated nonlinear measurement systems. We have shown that this approach can be used in various situations, including modeling of transistors for high-efficiency amplifier design [22] and modeling of the transistors' nonquasi static effects [23], [24].

In this paper, instead, we show that by properly acquiring and processing the dynamic-bias measurements, one can obtain the frequency-dependent S-parameters of a nonlinear device-under-test (DUT) across a time-varying large-signal operating point (LSOP). Interestingly, these time-varying S-parameters can be used in the same way as the conventional S-parameters for characterization, modeling, and design [13], [25]–[27].

This paper is organized as follows. In Section II, we discuss how the proposed technique to derive dynamic-bias S-parameters compares with similar existing approaches. In Section III, we describe how small-signal S-parameters are derived from the dynamic-bias measurements and the associated instrumentation setup. In Section IV, we report dynamic-bias S-parameters derived from simulation data of a CAD available nonlinear model on one hand and derived from the actual measurements of a GaAs transistor on the other hand. We also show that, in the case of a device where thermal and trapping effects are negligible, the dynamic-bias S-parameters coincide with the classical multibias

Manuscript received May 1, 2016; revised July 16, 2016 and August 30, 2016; accepted September 1, 2016. Date of publication September 28, 2016; date of current version November 3, 2016. The work of G. Avolio was supported by FWO Vlaanderen, Belgium.

G. Avolio and D. M. M.-P. Schreurs are with the Division ESAT-TELEMIC, Katholieke Universiteit Leuven, 3000 Leuven, Belgium (e-mail: gustavo.avolio@kuleuven.be).

A. Raffo, V. Vadalà, and G. Vannini are with the Department of Engineering, University of Ferrara, 44122 Ferrara, Italy.

Color versions of one or more of the figures in this paper are available online at http://ieeexplore.ieee.org.

Digital Object Identifier 10.1109/TMTT.2016.2608344

S-parameters that are measured with a vector network analyzer (VNA). Finally, we report characterization results for a GaN on SiC transistor in Section V.

II. Overview of Existing Techniques

In this section, we discuss how dynamic-bias S-parameters collocate with similar existing measurement techniques.

Dynamic-bias S-parameters belong to those measurement techniques consisting of exciting a nonlinear DUT with large- and small-signal excitations simultaneously [28]–[35]. In the context of nonlinear high-frequency circuits and devices, these techniques are employed to measure, among others, hot S-parameters and pulsed S-parameters.

In the case of hot S-parameters [30]–[33], which have laid the ground for the development of the more recently introduced X-parameters [36] and *S*-functions [37], the large- and small-signal excitations are CW signals. The large signal is applied at high frequency. The small signal is applied either at the same frequency of the large signal or at a different frequency [30], [31], [36]. As a result of hot S-parameter measurements, one obtains the nonlinear response of the DUT, as for example the AM/AM and AM/PM characteristics, and on top of that a set of power-dependent parameters describing the first-order approximation of the DUT perturbed around an LSOP very close to the actual operating condition. This set of parameters constitutes a very powerful behavioral description of weakly nonlinear DUTs, which, for example, interact with other blocks in a mismatched environment. The hot S_{22} [30]–[32], for instance, provides information on the DUT large-signal output mismatch. Although these parameters can be adopted in the description of the behavior of any nonlinear device, they are very suitable for mixers, amplifiers, and systems where these circuits are cascaded in.

Pulsed S-parameter measurements [34], [35], instead, are typically used for characterization of transistors experiencing slow memory effects. The large-signal excitation consists of bias pulses whose period and duty cycle allow one to control the thermal and traps-occupation states of the DUT. On top of the pulses, a high-frequency tickle is applied to measure the S-parameters at that fixed thermal state. The amplitude of the pulses determines the DUT-pulsed bias point around which S-parameters are measured. By controlling the pulses' amplitude and keeping fixed the period, the duty cycle, and the quiescent bias-point, one can gather isothermal and isodynamic S-parameters in various operating regions of the DUT [34]. Therefore, this technique is very powerful for characterizing dispersive effects as it actually allows to isolate trapping effects from thermal effects. In addition, if the transistor current is also measured within the pulse duration [34], [38]–[40], one can obtain pulsed IV characteristics. On the other hand, a pulsed LSOP is far from the actual operating conditions in many high-frequency circuits.

Dynamic-bias S-parameters position in between the two approaches described earlier. Similar to hot S-parameter measurements, they are derived by driving a nonlinear DUT with CW large and small excitations. However, differently from the hot S-parameter measurements, the frequency of the large-signal excitations is much lower than that of the small-signal excitations. This is a clear advantage, since the LSOP of the DUT is determined at much lower frequencies, namely, in the megahertz range where the hardware limitations, e.g., in terms of power, are more relaxed, and instruments' bandwidth is not an issue. On top of such a low-frequency LSOP, the small-signal excitation is simultaneously applied at the RF frequency of interest. Owing to the small power of the tickle, its harmonics can be neglected [21], and this enables the small-signal frequency to be set as high as the instrument bandwidth limit. Furthermore, one can straightforwardly set the LSOP very close to the actual transistor operation and exactly at the current-generator plane (e.g., class-F for high-efficiency amplifier). This is not obvious when the LSOP is set at higher frequencies, as is the case of hot S-parameter measurements, since nonlinear reactive effects and linear parasitics mask the actual temporal waveforms at the transistor current-generator plane. Importantly, and differently from hot S-parameters, the low-frequency LSOP represents a slowly varying bias point for the DUT. Therefore, we do not derive the dynamic-bias S-parameters as power-dependent perturbation quantities at the tickle frequency. We, instead, derive time-varying S-parameters by obtaining them around all the points of the time-varying LSOP and over the desired frequency range, as explained in Section III in more detail. This, definitely, constitutes an advantage also in comparison with pulsed S-parameters. Clearly, since the LSOP of dynamic-bias measurements is defined both by dc and low-frequency signals, each time we change it, both the thermal and traps-occupation states do change as well, and this represents the main difference with respect to pulsed measurements, where the trapping and thermal states are simply related to the selected bias condition.

In Section III, we explain how to derive dynamic-bias S-parameters.

III. Theoretical Background

As widely known, S-parameters for an active two-port network can be calculated, around a fixed bias point, by acquiring the network scattered waves as the result of two independent measurements obtained, for example, by applying a small-signal excitation first to port 1 and then to port 2. From these two measurements, one can straightforwardly derive the *S*-matrix

$$[\underline{S}] = \begin{bmatrix} b_{1,1} & b_{1,2} \\ b_{2,1} & b_{2,2} \end{bmatrix} \left(\begin{bmatrix} a_{1,1} & a_{1,2} \\ a_{2,1} & a_{2,2} \end{bmatrix} \right)^{-1} \tag{1}$$

where the second index indicates the port where the small-signal excitation is applied to. The scattered waves $b_{i,k}$ are complex numbers, which are unique for a given bias point (V_{dc}) and frequency (f_{RF})

$$b_{i,k} = |B_{i,k}(V_{\mathrm{dc}}, f_{\mathrm{RF}})| e^{j\left(2\pi f_{\mathrm{RF}} t + \varphi_{i,k}(V_{\mathrm{dc}}, f_{\mathrm{RF}})\right)}. \tag{2}$$

In this case, the dc bias voltages set a static operating point. Under dynamic-bias measurements, instead, low-frequency large-signal excitations at f_{LF} are superimposed on the dc voltages, thus determining a time-varying operating point [19]–[21], [28]–[33].

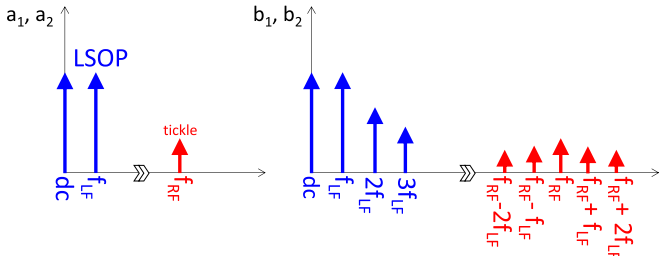

Fig. 1. Frequency spectra of the incident and scattered waves under dynamic-bias operation.

Similar to the classical small-signal measurements, a tickle at f_{RF} is applied first to port 1 and then to port 2 on top of the time-varying LSOP. As extensively discussed in [19]–[21], if the frequency of the LSOP f_{LF} is much smaller than f_{RF}, the LSOP can be assimilated as a slowly varying bias point as compared with the tickle. Moreover, if f_{LF} is selected above the cutoff frequency of dispersive effects and it is low enough to neglect reactive nonlinearities [14], the LSOP provides directly the device I–V characteristics at the thermal and trap states set by the LSOP itself.

Since the LSOP acts as a slowly varying bias point, it modulates the amplitude and the phase of the scattered waves at f_{RF}, which can be described by time-dependent complex numbers

$$b_{i,k} = |B_{i,k}(V(t),\, f_{RF})| e^{j(\varphi_{i,k}(V(t),f_{RF}))} e^{j(2\pi f_{RF} t)}. \quad (3)$$

If we were able to *freeze* the envelopes at a certain time instant t^*, we would reproduce a similar situation as described by (2), but with the bias point $V(t^*)$ applied dynamically and not statically. Clearly, if the device behavior manifested negligible low-frequency dynamic effects with respect to the LSOP, S-parameters derived from (1) by using either (2) or (3) should provide the same results, as we will demonstrate in Section IV. It is noteworthy that in (3), we refer only to the scattered waves assuming that the tickle applied to port 1 and port 2 is a pure CW small signal. When performing the actual dynamic-bias measurements, intermodulation tones around f_{RF} may appear also in the experimental incident waves due to mismatches between signal sources, measurement setup, and DUT. However, this does not affect at all the results as this is accounted for in (1) as in the case of standard S-parameters.

In order to derive small-signal parameters under dynamic-bias operation, the CW waves in (1) are replaced by the complex envelopes of the incident and scattered waves (3). These envelopes can be derived from the intermodulation tones induced around f_{RF} under dynamic-bias operation [19]–[21] and which are shown in Fig. 1 for illustrative purposes. As result of (1), one obtains an S-matrix that depends on f_{RF} and on the instantaneous dynamic-bias point $V(t^*)$ determined by the LSOP.

IV. Conceptual and Experimental Validation

A. Description of the Measurement Setup

In our previous works, we showed a measurement setup to perform dynamic-bias measurements based on a four-channel high-frequency sampler-based LSNA [4] extended with four additional channels to acquire synchronously also the low-frequency signals determining the LSOP. In this paper, we used a 10-MHz–67-GHz mixer-based LSNA [6], thus being able to measure both the LSOP and the intermodulation tones around f_{RF} with the same receivers. We customized the test set to perform dynamic-bias S-parameter measurements, as shown in Fig. 2. The couplers in front of the receivers have a high-pass characteristic in order to equalize the frequency components of the signals at the input and output ports of the DUT and prevent receivers' desensitization due to the presence of the large signals at low frequencies. The coupling factor is equal to 50 dB at 10 MHz and 15 dB at frequencies above 1 GHz. The diplexers and the bias-tees combine the dc and low- and high-frequency signals at the DUT plane. The LSOP is determined by the dc voltages and the low-frequency signals injected at the input and output ports. While the LSOP is turned ON, a high-frequency tickle is switched between port 1 and port 2, the other port being terminated with a passive load. For each LSOP, the frequency f_{RF} is swept, similar to small-signal measurements performed with a VNA.

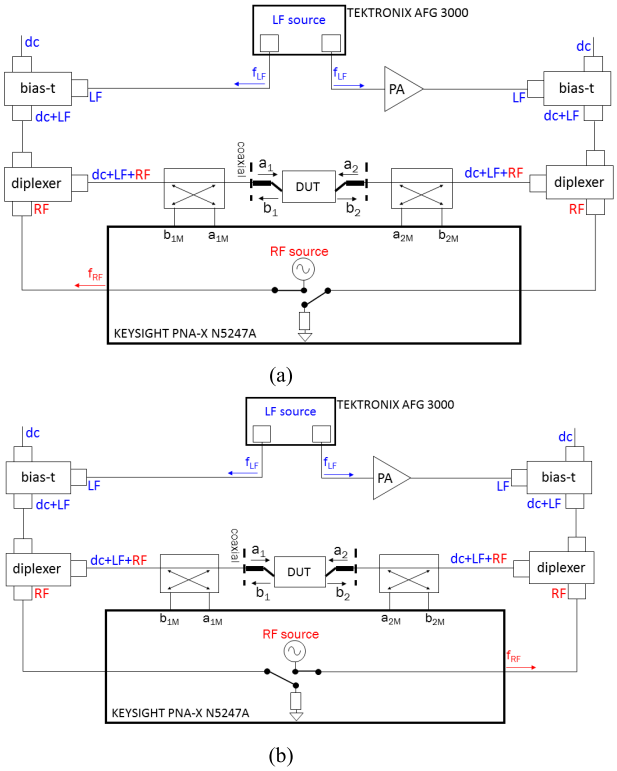

Fig. 2. Schematic of the setup adopted to measure dynamic-bias S-parameters. Tickle applied to (a) port 1 and (b) port 2.

The calibration of the setup consisted of a standard built-in procedure. First, we performed S-O-L, amplitude, and phase calibrations at the coaxial plane (Fig. 2) at the frequencies of interest. Next, we moved the reference plane at the on-wafer probe tips by performing a full two-port vector calibration.

B. Validation by Simulation and Experimental Data

In this section, we aim at demonstrating the validity of the proposed characterization technique by comparing the S-parameters obtained under dynamic-bias to classical multibias small-signal S-parameters. For this reason, we

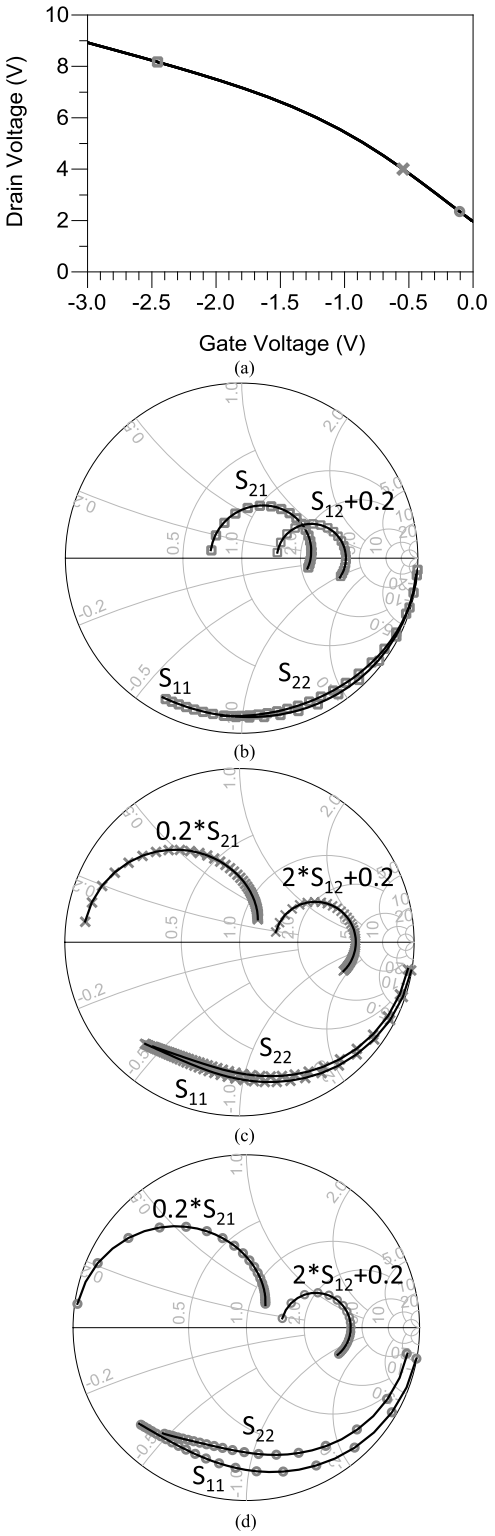

Fig. 3. (a) Simulated LSOP at $f_{\mathrm{LF}} = 10$ MHz, $V_{\mathrm{gdc}} = -1.5$ V, and $V_{\mathrm{ddc}} = 6$ V, and (b)–(d) simulated dynamic-bias S-parameters (symbols) from 1 to 40 GHz around the dynamic-bias points, which are marked on the LSOP trajectory in (a). Continuous lines in (b)–(d): classical S-parameters simulated by setting the dc voltages equal to those marked in (a). We used a CAD nonlinear model [41].

selected a CAD model and a DUT, which do not include and manifest any dispersive effect induced by the low-frequency LSOP. This implies that the dynamic-bias small-signal parameters and the classical small-signal parameters have to show the same behavior. In particular, for the simulation, we used a CAD available nonlinear transistor model for GaAs pHEMTs [41] implemented by adopting the nominal parameter values, whereas for the actual measurements, we used a 0.15-μm GaAs pHEMT.

In Fig. 3, we show the simulated LSOP [Fig. 3(a)] and the dynamic scattering (S-) parameters [Fig. 3(b)–(d)] for the CAD model. The LSOP was set at $V_{\mathrm{gdc}} = -1.5$ V, $V_{\mathrm{ddc}} = 6$ V, $A_g = 0.75$ V, and $A_d = 3$ V, with A_g and A_d being the amplitudes of the signal injected, respectively, at the gate and drain ports at $f_{\mathrm{LF}} = 10$ MHz. The relative phase between A_g and A_d was set equal to 180°. The power of the high-frequency tickle was set equal to -30 dBm and its frequency f_{RF} swept from 1 up to 40 GHz. Fig. 3(b)–(d) shows, in particular, the dynamic small-signal parameters (1) at three dynamic-points [$V_g(t^*)$ and $V_d(t^*)$] marked in Fig. 3(a). For the same device, we report in Fig. 3(b)–(d) also the classical small-signal parameters simulated by applying the dc voltages equal to those selected on the LSOP. As expected, the dynamic- and static-bias S-parameters coincide, confirming the theoretical assumptions we made in Section III.

To corroborate the proposed approach, we performed measurements on a GaAs transistor. GaAs technology is known to be very well established and manifesting very negligible trap-related dispersive effects. Moreover, we selected a device with small gate width in order to minimize the thermal effects. The LSOP [Fig. 4(a)] was applied at $f_{\mathrm{LF}} = 10$ MHz. The quiescent dc gate and drain voltages were $V_{\mathrm{gdc}} = -0.6$ V and $V_{\mathrm{ddc}} = 6$ V ($I_{\mathrm{ddc}} = 33$ mA). The amplitude of the incident wave at f_{LF} was 0.5 V, whereas the output low-frequency port was terminated with a passive load. The power of the tickle was set equal to -30 dBm, and f_{RF} was swept from 2 to 40 GHz. In Fig. 4(b) and (c), we report the amplitude of the measured envelopes at $f_{\mathrm{RF}} = 10$ GHz and with the tickle on port 1 [Fig. 4(b)] and port 2 [Fig. 4(c)]. The IF bandwidth of the measurements was 10 Hz to achieve the lowest noise level.

By applying (1) to the measured envelopes at each f_{RF}, one obtains the S-parameters, as a function of f_{RF}, at all the dynamic bias points of the LSOP in Fig. 4(a), as shown in Fig. 5.

For the same device, we measured also the classical multi-bias S-parameters with a VNA and compared them with the dynamic-bias S-parameters, as shown in Fig. 6. For the device considered in this paper, which had a relatively small size, we do not observe any significant difference between the conventional and dynamic-bias S-parameters. However, it is noteworthy that due to thermal effects, the two measurements do not have necessarily to agree, as the thermal state is clearly different in the two cases.

C. Comparison With a Sampler-Based LSNA

As we reported in [21], dynamic-bias measurements can be performed also with a sampler-based LSNA. The setup described in [21] is equipped with eight acquisition channels, four to acquire the low-frequency LSOP, and four to acquire the RF part of the frequency spectra. In this paper, we also

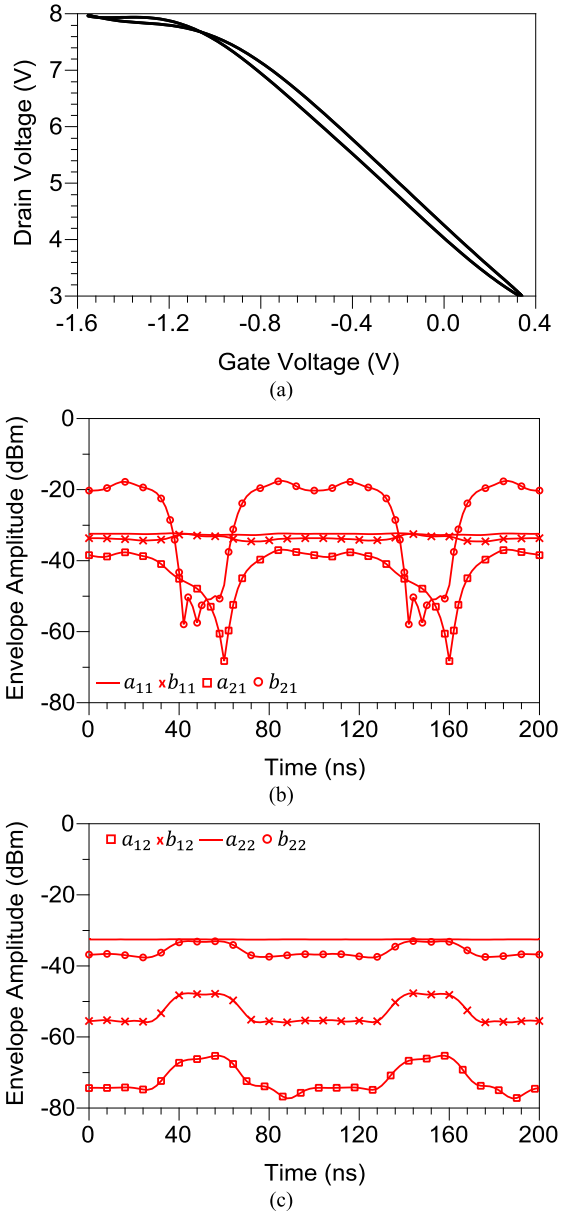

Fig. 4. (a) Measured LSOP and (b) and (c) envelopes around f_{RF}. (b) Envelopes when the tickle (a_{11}) is applied at port 1. (c) Envelopes when the tickle (a_{22}) is applied at port 2. $f_{LF} = 10$ MHz, $f_{RF} = 10$ GHz, $V_{gdc} = -0.6$ V, and $V_{ddc} = 6$ V. The DUT is a 0.15-μm GaAs pHEMT.

used that instrument to measure dynamic-bias S-parameters and compare them with those obtained from the measurements carried out with a mixer-based LSNA and reported in Section III. The DUT was the same 0.15-μm GaAs transistor. Moreover, with the sampler-based LSNA, we were able to change the frequency of the LSOP, as the low-frequency receivers enable the measurements below 10 MHz. In Fig. 7, we compare the dynamic-bias S-parameters measured with the sampler-based LSNA at $f_{LF} = 100$ kHz to those measured with the mixer-based LSNA at $f_{LF} = 10$ MHz. This result demonstrates that dynamic-bias S-parameter measurements could also be performed with a sampler-based LSNA, even though this instrument has a smaller dynamic range as compared with a mixer-based architecture. Indeed, since in the

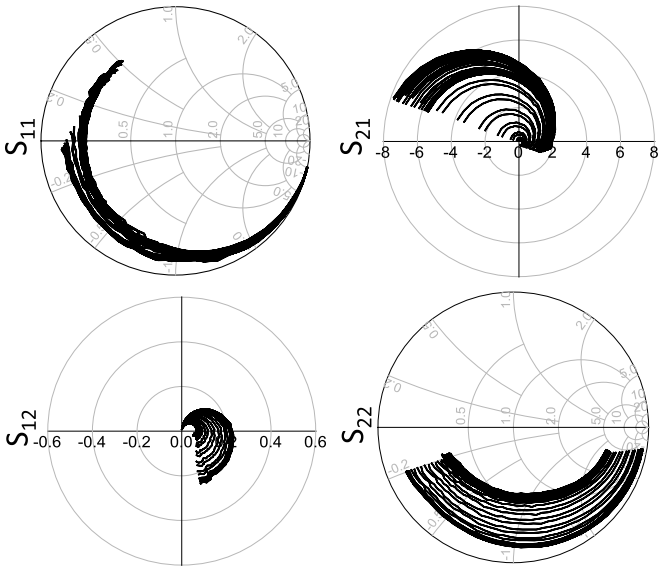

Fig. 5. Measured dynamic-bias S-parameters, derived from (1) and (3) as a function of frequency f_{RF} from 2 to 40 GHz and for all the dynamic-bias points corresponding to the LSOP at $f_{LF} = 10$ MHz in Fig. 4(a).

case of the sampler-based LSNA, the LSOP of the device is measured by separate receivers, the measurement sensitivity of the RF channels is high enough to ensure dynamic-bias S-parameter measurements with acceptable accuracy. In Fig. 7, measurements performed at two LSOP frequencies agree quite well, in line with the expectations for a technology manifesting negligible dispersion [42].

V. GaN Characterization

In this section, we report the characterization results for a 0.25-μm GaN on SiC transistor by using dynamic-bias S-parameters. Differently from the well-established GaAs technology, the GaN-based transistors are more prone to dispersive effects [38]–[40], [43], which mainly impact the transistor I–V characteristics and manifest as knee walkout and current collapse [14], [38]–[40]. In addition, low-frequency variation of small-signal parameters is a manifestation of dispersive effects, and it is typically captured by using either low-frequency VNA measurements [44] or pulsed S-parameter measurements [34], [35]. Dynamic-bias measurements, on the other hand, provide at the same time the dynamic I–V characteristics, which in fact coincide with the LSOP, and the small-signal parameters under large-signal operating condition and at the thermal and trap states set by the LSOP. Therefore, one can characterize the aforementioned effects because of the same measurement. In fact, the measured LSOP provides direct information on the effect of dispersion on the dynamic I–V characteristics. The small-signal parameters, measured along the time-varying LSOP, provide information on the effect of dispersion on high-frequency transistor behavior.

We performed the dynamic S-parameter measurements with the mixer-based LSNA. We changed the LSOP by varying the quiescent point and by actively tuning the load impedance at f_{LF}. The frequency f_{LF} was kept fixed at 10 MHz, which is above the cutoff frequency of the dispersive effects [14]. This implies that both the traps and temperature cannot follow the

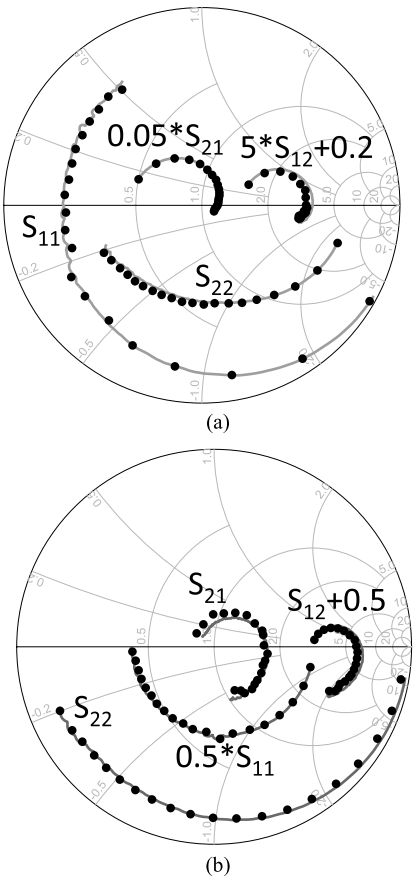

Fig. 6. Measured dynamic-bias S-parameters (black dots) and classical multibias (gray lines) S-parameters for a 0.15-μm GaAs pHEMT. The frequency of the LSOP is $f_{\mathrm{LF}} = 10$ MHz, and the bias point is $V_{\mathrm{gdc}} = -0.6$ V and $V_{\mathrm{ddc}} = 6$ V. The frequency f_{RF} of the tickle is swept from 2 to 40 GHz. (a) Dynamic bias point selected on the LSOP [Fig. 3(a)] is $V_g = -0.675$ V and $V_d = 6.69$ V, and the corresponding point selected on the multibias grid is $V_{\mathrm{gdc}} = -0.65$ V and $V_{\mathrm{ddc}} = 6.5$ V. (b) Dynamic point is $V_g = -1.53$ V and $V_d = 7.9$ V, and the corresponding point selected on the multibias grid is $V_{\mathrm{gdc}} = -1.5$ V and $V_{\mathrm{ddc}} = 8$ V.

time-varying LSOP, but remain frozen in a state determined by the bias point and by the shape of the load line. In fact, even if the bias point was fixed, the load line could instantaneously reach high-voltage regions, and this could further enhance traps filling [26], [40], [45]. In Fig. 8(a), we show the load lines corresponding to the measured LSOPs, and in Fig. 8(b) the dynamic-bias points corresponding to those load lines. In Fig. 8(a), we also report dc measurements for the same device. Fig. 8(a) provides us already with useful information on the device behavior. First, we can observe that, for all the load lines, the instantaneous current follows very similar trajectories from linear to saturation region, regardless of the quiescent point where the load lines were measured at and independently of the thermal and trap state, which is different for each load line. We only observe a slight difference between the static characteristic at $V_{\mathrm{gdc}} = 0$ V [Fig. 8(a) (black dots)] and the dynamic trajectory [Fig. 8(a) (dashed black line)] depicted by the low-frequency load lines. On the basis of these considerations, which can be readily derived as a result of the proposed measurement technique, the selected GaN transistor

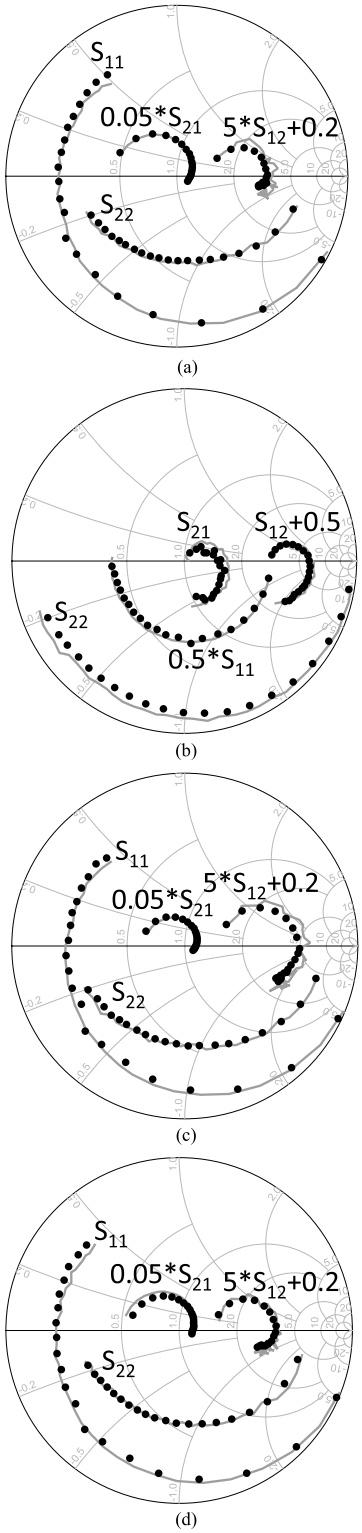

Fig. 7. Measured dynamic-bias S-parameters for a 0.15-μm GaAs pHEMT with a sampler-based LSNA at $f_{\mathrm{LF}} = 100$ kHz (gray line) and a mixer-based LSNA at $f_{\mathrm{LF}} = 10$ MHz (black dots). The dynamic bias points are (a) $V_g = -0.65$ V and $V_d = 6.4$ V, (b) $V_g = -1.4$ V and $V_d = 7.9$ V, (c) $V_g = -0.98$ V and $V_d = 7.5$ V, and (d) $V_g = 0.29$ V and $V_d = 3.1$ V. The frequency f_{RF} is swept from 2 to 40 GHz.

does not show significant dispersion in the I–V characteristics, and therefore, we do expect to observe a moderate dispersive behavior in the high-frequency small-signal parameters.

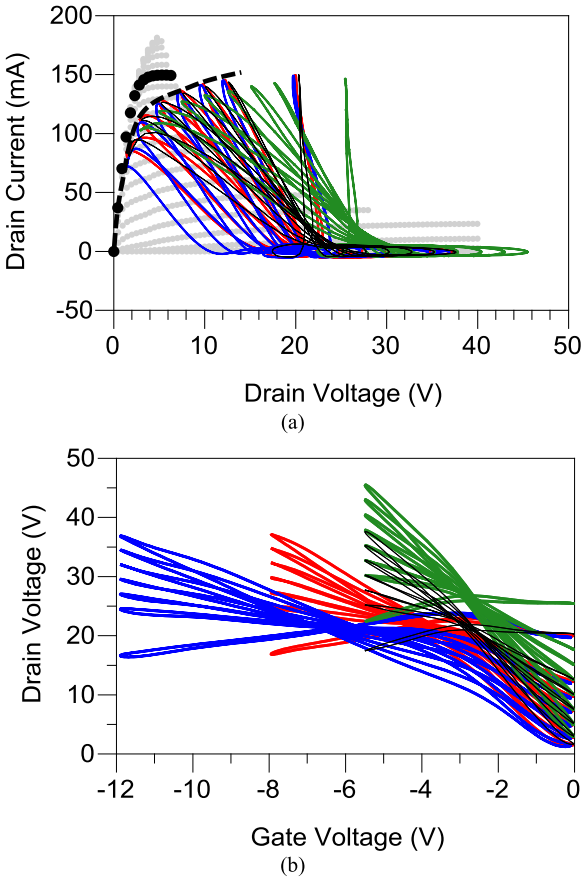

Fig. 8. Measured LSOPs of a 0.25-μm GaN on SiC HEMT transistor. (a) Load-lines and (b) corresponding dynamic-bias points at $f_{\rm LF} = 10$ MHz, $V_{\rm gdc} = -2.75$ V and $V_{\rm ddc} = 20$ V (black continuous line), $V_{\rm gdc} = -2.75$ V and $V_{\rm ddc} = 25$ V (green lines in color version), $V_{\rm gdc} = -4$ V and $V_{\rm ddc} = 20$ V (red lines in color version), and $V_{\rm gdc} = -6$ V and $V_{\rm ddc} = 20$ V (blue lines in color version). For each bias point, the load was swept by active injection. In (a), we report also the measured dc characteristics (gray symbols). The dc characteristic at $V_{\rm gdc} = 0$ V (black dots) and the dynamic trajectory at $V_g = 0$ V (dashed black line) are also highlighted in (a).

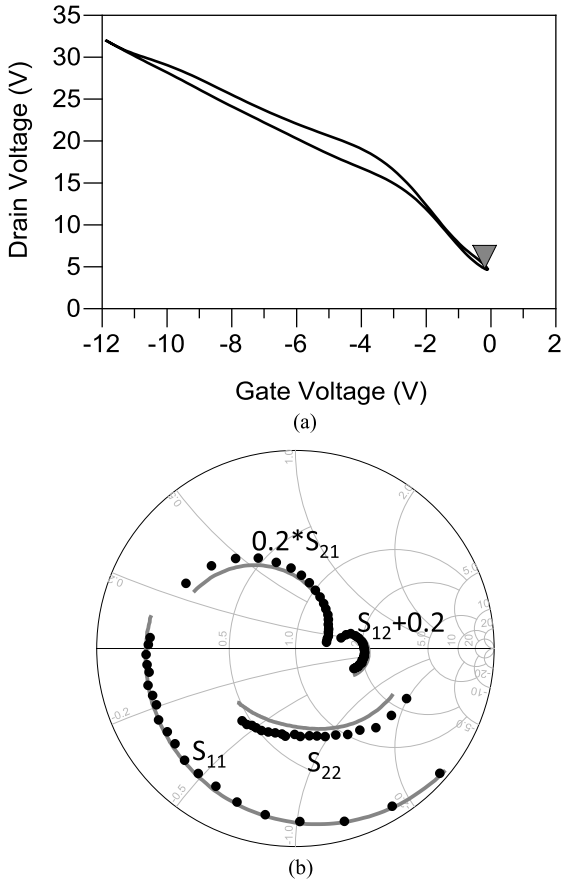

Fig. 9. (a) Measured input–output LSOP trajectory for a 0.25-μm GaN on SiC HEMT transistor at $f_{\rm LF} = 10$ MHz, $V_{\rm gdc} = -6$ V, and $V_{\rm ddc} = 20$ V. (b) Dynamic S-parameters as a function of $f_{\rm RF}$ from 2 to 20 GHz around the dynamic point, indicated in (a) with triangle symbol, $V_g = -0.2$ V and $V_d = 4.7$ V (black symbols). Classical S-parameters measured with a VNA at $V_{\rm gdc} = -0.2$ V and $V_{\rm ddc} = 4.7$ V (gray line).

We measured dynamic S-parameters, on top of each load line in Fig. 8(a), by sweeping the tickle frequency $f_{\rm RF}$ from 1 to 20 GHz with the tickle power set equal to -30 dBm. The IF bandwidth was set equal to 1 kHz, which represented an acceptable tradeoff between measurement time and noise level for the measurements that we performed. Next, we derived envelopes from the measured RF intermodulation tones and use them to compute the dynamic-bias S-matrix by (1). As a result, we obtained the S-parameters at each dynamic point in Fig. 8(b) and as a function of $f_{\rm RF}$.

In Fig. 9, we show the dynamic-bias S-parameters at a point in the linear region on one of the load lines measured at $V_{\rm gdc} = -6$ V and $V_{\rm ddc} = 20$ V. The input–output trajectory corresponding to the selected load line is reported in Fig. 9(a). On that trajectory, we selected the dynamic point at $V_g = -0.2$ V and $V_d = 4.7$ V, which is marked in Fig. 9(a). In Fig. 9(b), we show the dynamic-bias S-parameters (black symbols) and the S-parameters measured with a VNA (gray line) with the device statically biased at $V_{\rm gdc} = -0.2$ V and $V_{\rm ddc} = 4.7$ V. In Fig. 9(b), we clearly observe a difference between static and dynamic-bias S_{22}. The in-depth understanding of the physical origin of this discrepancy is outside the scope of this paper. However, an intuitive explanation can be given by considering that, as $f_{\rm RF}$ decreases, S_{22} becomes directly linked to the transistor small-signal output conductance (g_d) or the Y_{22} parameter, which is the ac slope of the IV output characteristics at low frequencies. For the static bias measurement, the ac slope is measured at the thermal and trap states determined by dc voltages. On the other hand, under dynamic-bias conditions, the ac slope is measured at the thermal and trap states set by the low-frequency LSOP, which are different from those determined by a static bias. It is also noteworthy that the parameter S_{11}, which is directly linked to the transistor input capacitance, is practically identical in the two cases. This is coherent with the fact that, as experimentally demonstrated in many works, low-frequency dispersion has second order effects on transistor capacitances [5], [15], [19]–[22].

In Fig. 10, we compare, instead, the dynamic-bias S-parameters around the same dynamic point, but on two LSOPs. In particular, we selected the dynamic point $V_g = -1$ V and $V_d = 12$ V on two load lines whose input–output trajectories are shown in Fig. 10(a) and measured at $V_{\rm gdc} = -2.75$ V, $V_{\rm ddc} = 20$ V [Fig. 10(a) (gray line)], and

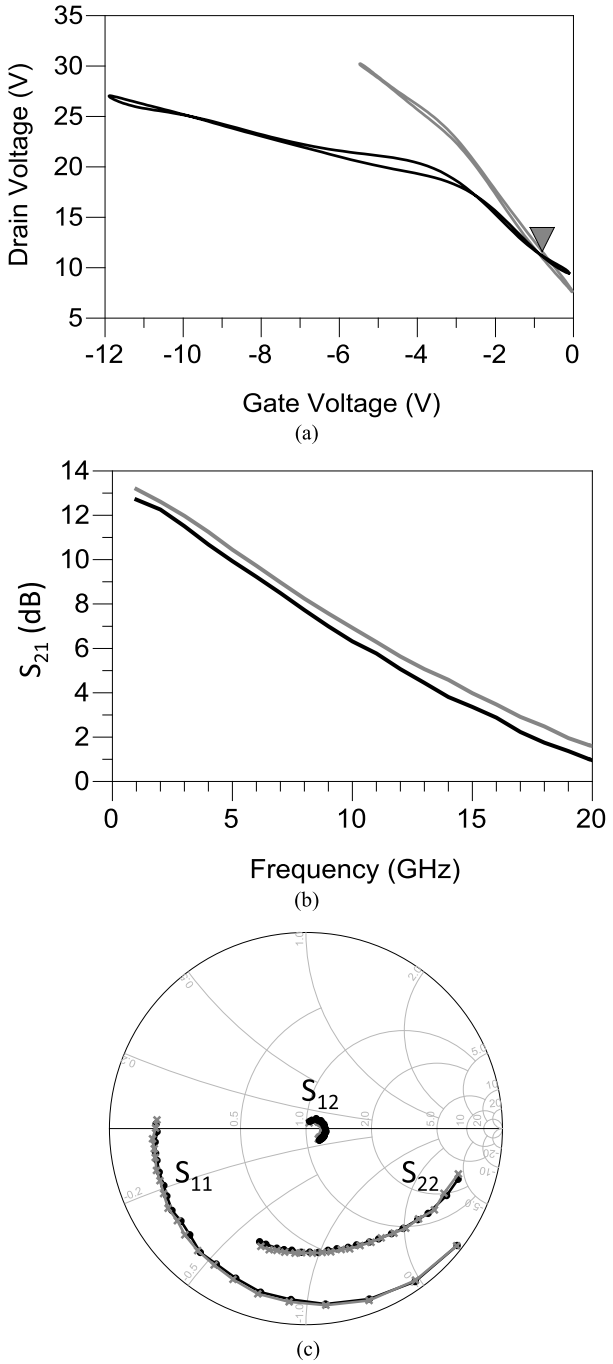

Fig. 10. (a) Measured input–output LSOP trajectories for a 0.25-μm GaN on SiC HEMT transistor at $f_{\mathrm{LF}} = 10$ MHz, $V_{\mathrm{gdc}} = -6$ V and $V_{\mathrm{ddc}} = 20$ V (black line), and $V_{\mathrm{gdc}} = -2.75$ V and $V_{\mathrm{ddc}} = 20$ V (gray line). (b) and (c) Dynamic S-parameters as a function of f_{RF} from 2 to 20 GHz around the dynamic point, indicated in (a) with triangle symbol, $V_g = -1$ V and $V_d = 12$ V.

$V_{\mathrm{gdc}} = -6$ V and $V_{\mathrm{ddc}} = 20$ V [Fig. 10(a) (black line)]. As expected, the dynamic-bias parameters S_{11} and S_{12} do not exhibit any difference with respect to the LSOP. We observe a slight shift of the parameter S_{21}. Such a deviation is related to the different trap state associated with the two LSOPs that, as expected, causes a lower gain at lower V_{gdc}. In addition, the drop of S_{21} as V_{gdc} decreases cannot be ascribed in this case to the slightly different thermal state determined by the average dissipated power across the two load lines, which was 545 mW for the load line at $V_{\mathrm{gdc}} = -2.75$ V and 397 mW for the load line at $V_{\mathrm{gdc}} = -6$ V. If the drop were due to thermal effects, we should expect the S_{21} on top of the load line corresponding to the higher dissipated power to be lower than the S_{21} on top of the other load line. As regarding the parameters and S_{22}, we do not observe any significant shift in the two cases, especially at lower frequencies where this parameter is directly linked to the slope of the device output characteristics, which in turn determines the device output impedance. Since the selected dynamic-bias point ($V_g = -1$ V and $V_d = 12$ V) lays in saturation region where the slope of the output characteristics is very low, the resulting device output impedance, which is linked to S_{22}, is quite high and slightly sensitive to the changes in traps and thermal state.

We want to highlight once again that the proposed measurement technique enables a more extensive study of dispersive effects by looking at the same time at the transistor dynamic I–V characteristics and at the high-frequency small-signal parameters across a realistic LSOP.

Furthermore, for a fixed LSOP, as in the case of high-efficiency power-amplifiers, one can obtain the S-parameters at all the points of the LSOP and use them in the design phase [13], [25], [27]. Finally, although the proposed technique does not provide information on the actual traps and thermal states, by performing dynamic bias-measurements at different LSOPs, one can obtain a data set, which can then be used to extract a nonlinear transistor model including dispersive effects as, for example, the one proposed in [15].

VI. Conclusion

We described a novel technique to obtain the scattering (S-) parameters of microwave transistors under large-signal operating conditions. The peculiarity of this measurement technique consists in providing at once the load line at the transistor current-source, which coincides with the LSOP and is measured at low frequencies, and at the same time, the high-frequency S-parameters along that load line. It relies on the dynamic-bias approach and, differently from classical multibias S-parameters, the DUT S-parameters are measured at all the dynamic-bias points of a time-varying LSOP. Interestingly, these time-varying S-parameters can be used similarly as the conventional S-parameters for characterization and modeling purposes, as they carry a great deal of information, especially when dealing with the transistors whose behavior is affected by low-frequency dispersion.

Acknowledgment

Authors G. Avolio and D. M. M.-P. Schreurs would like to thank the Hercules Foundation.

References

[1] U. Lott, "Measurement of magnitude and phase of harmonics generated in nonlinear microwave two-ports," *IEEE Trans. Microw. Theory Techn.*, vol. 37, no. 10, pp. 1506–1511, Oct. 1989.

[2] G. Kompa and F. V. Raay, "Error-corrected large-signal waveform measurement system combining network analyzer and sampling oscilloscope capabilities," *IEEE Trans. Microw. Theory Techn.*, vol. 38, no. 4, pp. 358–365, Apr. 1990.

[3] A. Ferrero and U. Pisani, "An improved calibration technique for on-wafer large-signal transistor characterization," *IEEE Trans. Instrum. Meas.*, vol. 42, no. 2, pp. 360–364, Apr. 1993.

[4] T. V. D. Broeck and J. Verspecht, "Calibrated vectorial nonlinear-network analyzers," in *IEEE MTT-S Int. Microw. Symp. Dig.*, vol. 2. May 1994, pp. 1069–1072.

[5] M. C. Curras-Francos, P. J. Tasker, M. Fernandez-Barciela, Y. Campos-Roca, and E. Sanchez, "Direct extraction of nonlinear FET Q-V functions from time domain large signal measurements," *IEEE Microw. Guided Wave Lett.*, vol. 10, no. 12, pp. 531–533, Dec. 2000.

[6] P. Blockley, D. Gunyan, and J. B. Scott, "Mixer-based, vector-corrected, vector signal/network analyzer offering 300 kHz–20 GHz bandwidth and traceable phase response," in *IEEE MTT-S Int. Microw. Symp. Dig.*, Jun. 2005, pp. 1497–1500.

[7] D. Williams, P. Hale, and K. A. Remley, "The sampling oscilloscope as a microwave instrument," *IEEE Microw. Mag.*, vol. 8, no. 4, pp. 59–68, Aug. 2007.

[8] M. Marchetti, M. J. Pelk, K. Buisman, W. C. E. Neo, M. Spirito, and L. C. N. D. Vreede, "Active harmonic load–pull with realistic wideband communications signals," *IEEE Trans. Microw. Theory Techn.*, vol. 56, no. 12, pp. 2979–2988, Dec. 2008.

[9] H. Qi, J. Benedikt, and P. J. Tasker, "Nonlinear data utilization: From direct data lookup to behavioral modeling," *IEEE Trans. Microw. Theory Techn.*, vol. 57, no. 6, pp. 1425–1432, Jun. 2009.

[10] P. Roblin, D. E. Root, J. Verspecht, Y. Ko, and J. P. Teyssier, "New trends for the nonlinear measurement and modeling of high-power RF transistors and amplifiers with memory effects," *IEEE Trans. Microw. Theory Techn.*, vol. 60, no. 6, pp. 1964–1978, Jun. 2012.

[11] V. Vadalà, A. Raffo, S. Di Falco, G. Bosi, A. Nalli, and G. Vannini, "A load–pull characterization technique accounting for harmonic tuning," *IEEE Trans. Microw. Theory Techn.*, vol. 61, no. 7, pp. 2695–2704, Jul. 2013.

[12] V. Teppati *et al.*, "A *W*-band on-wafer active load-pull system based on down-conversion techniques," *IEEE Trans. Microw. Theory Techn.*, vol. 62, no. 1, pp. 148–153, Jan. 2014.

[13] A. Raffo, F. Scappaviva, and G. Vannini, "A new approach to microwave power amplifier design based on the experimental characterization of the intrinsic electron-device load line," *IEEE Trans. Microw. Theory Techn.*, vol. 57, no. 7, pp. 1743–1752, Jul. 2009.

[14] A. Raffo, S. Di Falco, V. Vadalà, and G. Vannini, "Characterization of GaN HEMT low-frequency dispersion through a multiharmonic measurement system," *IEEE Trans. Microw. Theory Techn.*, vol. 58, no. 9, pp. 2490–2496, Sep. 2010.

[15] A. Raffo *et al.*, "Nonlinear dispersive modeling of electron devices oriented to GaN power amplifier design," *IEEE Trans. Microw. Theory Techn.*, vol. 58, no. 4, pp. 710–718, Apr. 2010.

[16] G. Pailloncy, G. Avolio, M. Myslinski, Y. Rolain, M. V. Bossche, and D. Schreurs, "Large-signal network analysis including the baseband," *IEEE Microw. Mag.*, vol. 12, no. 2, pp. 77–86, Apr. 2011.

[17] J. Xu, R. Jones, S. A. Harris, T. Nielsen, and D. E. Root, "Dynamic FET model—DynaFET—For GaN transistors from NVNA active source injection measurements," in *IEEE Int. MTT-S Microw. Symp. Dig.*, Jun. 2014, pp. 1–3.

[18] S. Schafer and Z. Popović, "Multi-frequency measurements for supply modulated transmitters," *IEEE Trans. Microw. Theory Techn.*, vol. 63, no. 9, pp. 2931–2941, Sep. 2015.

[19] G. Avolio *et al.*, "Nonlinear model for 40-GHz cold-FET operation," in *Proc. IEEE Int. Workshop Integr. Nonlinear Microw. Millim.-Wave Circuits*, Apr. 2014, pp. 1–3.

[20] V. Vadalà, A. Raffo, G. Vannini, G. Avolio, and D. M. M. P. Schreurs, "GaN HEMT model extraction based on dynamic-bias measurements," in *Proc. Eur. Microw. Integr. Circuit Conf. (EuMIC)*, Oct. 2014, pp. 206–209.

[21] G. Avolio *et al.*, "Millimeter-wave FET nonlinear modelling based on the dynamic-bias measurement technique," *IEEE Trans. Microw. Theory Techn.*, vol. 62, no. 11, pp. 2526–2537, Nov. 2014.

[22] V. Vadalà, A. Raffo, G. Avolio, M. Marchetti, D. M. M.-P. Schreurs, and G. Vannini, "Extraction of accurate GaN HEMT model for high-efficiency power amplifier design," in *IEEE Int. MTT-S Microw. Symp. Dig.*, May 2015, pp. 1–4.

[23] G. Crupi, D. M. M.-P. Schreurs, A. Caddemi, A. Raffo, and G. Vannini, "Investigation on the non-quasi-static effect implementation for millimeter-wave FET models," *Int. J. RF Microw., Comput.-Aided Eng.*, vol. 20, no. 1, pp. 87–93, Jan. 2010.

[24] A. Raffo, G. Avolio, V. Vadalà, D. M. M.-P. Schreurs, and G. Vannini, "A non-quasi-static FET model extraction procedure using the dynamic-bias technique," *IEEE Microw. Wireless Compon. Lett.*, vol. 25, no. 12, pp. 841–843, Dec. 2015.

[25] H. Jang, P. Roblin, and Z. Xie, "Model-based nonlinear embedding for power-amplifier design," *IEEE Trans. Microw. Theory Techn.*, vol. 62, no. 9, pp. 1986–2002, Sep. 2014.

[26] A. Raffo, G. Bosi, V. Vadalà, and G. Vannini, "Behavioral modeling of GaN FETs: A load-line approach," *IEEE Trans. Microw. Theory Techn.*, vol. 62, no. 1, pp. 73–82, Jan. 2014.

[27] P. Roblin, H.-C. Chang, F. J. Martinez-Rodriguez, C. Xie, and J. I. Martinez-Lopez, "On the design of GaN chireix power amplifiers using an embedding device model," *Int. J. Numer. Model., Electron. Netw., Devices Fields*, to be published, doi: 10.1002/jnm.2148.2016.

[28] F. Verbeyst and M. V. Bossche, "VIOMAP, the S-parameter equivalent for weakly nonlinear RF and microwave devices," in *IEEE MTT-S Int. Microw. Symp. Dig.*, May 1994, pp. 1369–1372.

[29] J. Martens and P. Kapetanic, "Probe-tone S-parameter measurements," *IEEE Trans. Microw. Theory Techn.*, vol. 50, no. 9, pp. 2076–2082, Sep. 2002.

[30] T. Gasseling, D. Barataud, S. Mons, J. M. Nebus, J. P. Villotte, and R. Quere, "A new characterization technique of 'four hot S parameters' for the study of nonlinear parametric behaviors of microwave devices," in *IEEE MTT-S Int. Microw. Symp. Dig.*, Jun. 2003, pp. 1663–1666.

[31] T. Gasseling *et al.*, "Hot small-signal S-parameter measurements of power transistors operating under large-signal conditions in a load-pull environment for the study of nonlinear parametric interactions," *IEEE Trans. Microw. Theory Techn.*, vol. 52, no. 3, pp. 805–812, Mar. 2004.

[32] J. Verspecht, D. Barataud, J. P. Teyssier, and J. M. Nébus, "Hot S-parameter techniques: $6 = 4+2$," in *Proc. 66th ARFTG Conf.*, pp. 1–9, Dec. 2005.

[33] J. Verspecht, D. F. Williams, D. Schreurs, K. A. Remley, and M. D. McKinley, "Linearization of large-signal scattering functions," *IEEE Trans. Microw. Theory Techn.*, vol. 53, no. 4, pp. 1369–1376, Apr. 2005, doi: 10.1109/TMTT.2005.845771.

[34] J.-P. Teyssier, P. Bouysse, Z. Ouarch, D. Barataud, T. Peyretaillade, and R. Quere, "40-GHz/150-ns versatile pulsed measurement system for microwave transistor isothermal characterization," *IEEE Trans. Microw. Theory Techn.*, vol. 46, no. 12, pp. 2043–2052, Dec. 1998.

[35] J. Martens, "Pulsed S-parameter measurements: On resolution, duration, and uncertainty," in *Proc. IEEE Int. Conf. Microw., Commun., Antennas Electron. Syst.*, Oct. 2013, pp. 1–5.

[36] J. Verspecht and D. E. Root, "Polyharmonic distortion modeling," *IEEE Microw. Mag.*, vol. 7, no. 3, pp. 44–57, Jun. 2006.

[37] M. Myslinski, F. Verbeyst, M. V. Bossche, and D. Schreurs, "S-functions behavioral model order reduction based on narrowband modulated large-signal network analyzer measurements," in *Proc. 75th Microw. Meas. Conf. (ARFTG)*, May 2010, pp. 1–6.

[38] A. E. Parker and J. G. Rathmell, "Measurement and characterization of HEMT dynamics," in *Proc. Asia–Pacific Microw. Conf.*, Dec. 2000, pp. 846–849.

[39] O. Jardel *et al.*, "An electrothermal model for AlGaN/GaN power HEMTs including trapping effects to improve large-signal simulation results on high VSWR," *IEEE Trans. Microw. Theory Techn.*, vol. 55, no. 12, pp. 2660–2669, Dec. 2007.

[40] A. Santarelli *et al.*, "GaN FET nonlinear modeling based on double pulse *I/V* characteristics," *IEEE Trans. Microw. Theory Techn.*, vol. 62, no. 12, pp. 3262–3273, Dec. 2014.

[41] I. Angelov, N. Rorsman, J. Stenarson, M. Garcia, and H. Zirath, "An empirical table-based FET model," *IEEE Trans. Microw. Theory Techn.*, vol. 47, no. 12, pp. 2350–2357, Dec. 1999.

[42] G. Avolio, D. Schreurs, B. Nauwelaers, A. Raffo, G. Vannini, and G. Crupi, "Bias and frequency dispersion of dynamic I-V characteristics in microwave transistors," in *Proc. Eur. Microw. Integr. Circuits Conf. (EuMIC)*, Oct. 2011, pp. 93–96.

[43] V. I. Cojocaru and T. J. Brazil, "A scalable general-purpose model for microwave FETs including DC/AC dispersion effects," *IEEE Trans. Microw. Theory Techn.*, vol. 45, no. 12, pp. 2248–2255, Dec. 1997.

[44] J. C. Nallatamby, R. Sommet, S. Laurent, M. Prigent, R. Quere, and O. Jardel, "A microwave modeling oxymoron?: Low-frequency measurements for microwave device modeling," *IEEE Microw. Mag.*, vol. 15, no. 4, pp. 92–107, Jun. 2014.

[45] A. S. Roy and C. C. Enz, "Analytical modeling of large-signal cyclo-stationary low-frequency noise with arbitrary periodic input," *IEEE Trans. Electron Devices*, vol. 54, no. 9, pp. 2537–2545, Sep. 2007.

Gustavo Avolio (M'12) was born in Cosenza, Italy, in 1982. He received the M.Sc. degree in electronic engineering from the University of Calabria, Cosenza, in 2006, and the Ph.D. degree in electronic engineering from the Katholieke Universiteit Leuven, Leuven, Belgium.

He is currently a Post-Doctoral Researcher supported by FWO Vlaanderen, Belgium. In 2013 and 2014, he has been a Visiting Scientist with the National Institute of Standards and Technology, Boulder, CO, USA. Since 2009, he has often been a Visiting Scientist with the University of Ferrara, Ferrara, Italy. His current research interests include large-signal measurements and nonlinear modeling of advanced microwave devices.

Antonio Raffo (S'04–M'07) was born in Taranto, Italy, in 1976. He received the M.S. degree (Hons.) in electronic engineering and the Ph.D. degree in information engineering from the University of Ferrara, Ferrara, Italy, in 2002 and 2006, respectively.

Since 2002, he has been with the Engineering Department, University of Ferrara, where he is currently a Research Associate and teaches courses in semiconductor devices and electronic instrumentation and measurement. His current research interests include nonlinear electron device characterization and the modeling and circuit-design techniques for nonlinear microwave and millimeter-wave applications. He has co-authored over 100 publications in international journals and conferences and co-edited *Microwave Wireless Communications: From Transistor to System Level* (Oxford, U.K.: Elsevier, 2016).

Dr. Raffo is a member of the Technical Programme Committee of the IEEE International Workshop on Integrated Nonlinear Microwave and Millimetre-wave Circuits (INMMiC) and the IEEE Microwave Measurement Technical Committee (MTT-11). He serves as an Associate Editor for the *International Journal of Numerical Modelling: Electronic Networks, Devices and Fields*, and was the Technical Programme Committee Chair of the IEEE INMMiC Conference, Leuven, Belgium, 2014.

Valeria Vadalà (S'07–M'11) was born in Reggio Calabria, Italy, in 1982. She received the M.S. degree (Hons.) in electronic engineering from the Mediterranea University of Reggio Calabria, Reggio Calabria, in 2006, and the Ph.D. degree in information engineering from the University of Ferrara, Ferrara, Italy, in 2010.

She is currently with the Department of Engineering, University of Ferrara, as a Post-Doctoral Researcher. Her current research interests include nonlinear electron-device characterization and the modeling and circuit-design techniques for nonlinear microwave and millimeter-wave applications.

Giorgio Vannini (S'87–M'92) received the Laurea degree in electronic engineering and the Ph.D. degree in electronic and computer science engineering from the University of Bologna, Bologna, Italy.

In 1993, he joined the Department of Electronics, University of Bologna, as a Research Associate. From 1994 to 1998, he was with the Research Centre on Electronics, Computer Science and Telecommunication Engineering, National Research Council, Bologna, where he was responsible for MMIC testing and the Computer-Aided Design Laboratory. In 1998, he joined the University of Ferrara, Ferrara, Italy, as an Associate Professor, where he has been a Full Professor of electronics since 2005. He was the Head of the Engineering Department from 2007 to 2015. He is the co-founder of the academic spinoff Microwave Electronics for Communications. During his academic career, he has coauthored over 250 papers devoted to electron device modeling, the computer-aided design techniques for MMICs, and nonlinear circuit analysis and design.

Dominique M. M.-P. Schreurs (S'90–M'97–SM'02–F'12) received the M.Sc. degree in electronic engineering and the Ph.D. degree from the Katholieke Universiteit Leuven, Leuven, Belgium.

She is currently a Full Professor with the Katholieke Universiteit Leuven. She has been a Visiting Scientist with Agilent Technologies, Santa Rosa, CA, USA, ETH Zürich, Zürich, Switzerland, and the National Institute of Standards and Technology, Boulder, CO, USA. Her main research interests concern the (non)linear characterization and modeling of active microwave devices, and (non)linear circuit design for telecommunications and biomedical applications.

Dr. Schreurs serves on the AdCom of the MTT Society and also serves as an Editor-in-Chief for the IEEE TRANSACTIONS ON MICROWAVE THEORY AND TECHNIQUES and as the Vice-President on the Executive Committee of the ARFTG organization. She was the General Chair of the 2007 and 2012 Spring ARFTG Conference and the Co-Chair of the European Microwave Conference in 2008. She was an MTT-S Distinguished Microwave Lecturer.